Hydrocarbon double-stapling remedies the proteolytic instability of a lengthy peptide therapeutic

Gregory H. Bird[a,b], Navid Madani[c,d], Alisa F. Perry[a,b], Amy M. Princiotto[c], Jeffrey G. Supko[e], Xiaoying He[e], Evripidis Gavathiotis[a,b], Joseph G. Sodroski[c,f], and Loren D. Walensky[a,b,1]

[a]Department of Pediatric Oncology, Dana–Farber Cancer Institute and Children's Hospital Boston, Harvard Medical School, Boston, MA 02115; [b]Program in Cancer Chemical Biology, Dana–Farber Cancer Institute, Boston, MA 02115; [c]Department of Cancer Immunology and AIDS, Dana–Farber Cancer Institute, Division of AIDS, Harvard Medical School, Boston, MA 02115; [d]Department of Pathology, Harvard Medical School, Boston, MA 02115; [e]Clinical Pharmacology Laboratory, Department of Medicine, Massachusetts General Hospital, Boston, MA 02114; and [f]Department of Immunology and Infectious Diseases, Harvard School of Public Health, Boston, MA 02115

Edited* by Solomon H. Snyder, Johns Hopkins University School of Medicine, Baltimore, MD, and approved June 18, 2010 (received for review March 3, 2010)

The pharmacologic utility of lengthy peptides can be hindered by loss of bioactive structure and rapid proteolysis, which limits bioavailability. For example, enfuvirtide (Fuzeon, T20, DP178), a 36-amino acid peptide that inhibits human immunodeficiency virus type 1 (HIV-1) infection by effectively targeting the viral fusion apparatus, has been relegated to a salvage treatment option mostly due to poor in vivo stability and lack of oral bioavailability. To overcome the proteolytic shortcomings of long peptides as therapeutics, we examined the biophysical, biological, and pharmacologic impact of inserting all-hydrocarbon staples into an HIV-1 fusion inhibitor. We find that peptide double-stapling confers striking protease resistance that translates into markedly improved pharmacokinetic properties, including oral absorption. We determined that the hydrocarbon staples create a proteolytic shield by combining reinforcement of overall α-helical structure, which slows the kinetics of proteolysis, with complete blockade of peptide cleavage at constrained sites in the immediate vicinity of the staple. Importantly, double-stapling also optimizes the antiviral activity of HIV-1 fusion peptides and the antiproteolytic feature extends to other therapeutic peptide templates, such as the diabetes drug exenatide (Byetta). Thus, hydrocarbon double-stapling may unlock the therapeutic potential of natural bioactive polypeptides by transforming them into structurally fortified agents with enhanced bioavailability.

fusion inhibitor | HIV-1 | protease resistance | stapled peptide | alpha-helix

Harnessing bioactive peptides to develop highly selective and potent pharmacologic agents for targeting pathologic proteins and their interactions remains an appealing strategy for drug discovery. Despite the allure of applying "nature's solution" to protein targeting, peptides are typically administered by injection because of their inherently poor oral bioavailability and they are rapidly cleared as a consequence of peptidase-mediated metabolism. Nevertheless, therapeutic antibodies, enzymes, hormones, and other peptides, whose chemical architecture is based on the amide bond, represent an essential and growing component of the pharmaceutical repertoire. By inserting an all-hydrocarbon "staple" within short peptide sequences (1–3), we previously developed stabilized alpha helices (SAH) of BCL-2 domains (4, 5) and p53 (6) that exhibit sturdy α-helical structure, protease resistance, cell penetrance, and targeted biological activity. Here, we explored the potential of hydrocarbon double-stapling to structurally fortify lengthy bioactive peptides and remedy their proteolytic vulnerability in vitro and in vivo. We chose the peptidic fusion inhibitors of human immunodeficiency virus type 1 (HIV-1) as the template for our study because their biophysical shortcomings reflect the practical challenges for broader application of lengthy peptide therapeutics.

Enfuvirtide, the first fusion inhibitor shown to block HIV-1 entry in humans, is a decoy α-helix that disrupts assembly of the six-helix bundle viral fusion apparatus by mimicking the heptad repeat 2 (HR2) oligomerization domain of the gp41 envelope glycoprotein (7) (Fig. 1*A*). A wide variety of viral families rely on this helical bundle assembly mechanism to infect host cells, highlighting the potential of this pharmacologic strategy to yield both preventive and suppressive antiviral agents (8, 9). Despite successful validation of this targeted anti-HIV-1 therapy in humans (7), enfuvirtide has remained a treatment option of last resort mostly due to cost, lack of oral bioavailability, accelerated systemic clearance from in vivo proteolysis, and the development of drug resistance (10, 11). Whereas peptide-based inhibition of viral fusion is mechanistically feasible and clinically effective, the biophysical, biological, and pharmacologic liabilities of fusion-inhibiting peptides have thwarted their optimal therapeutic application.

We sought to optimize HIV-1 fusion inhibitor peptides by generating SAH of gp41 (SAH-gp41) through all-hydrocarbon covalent crosslinking of a variant of T649 (628–663), which we refer to as T649v (626–662). T649 peptides contain conserved HIV-1 gp41 residues that contribute to the stability of the six-helix bundle and thus exhibit improved antiviral potency compared to enfuvirtide (638–673) (12). Because the intramolecular binding interfaces of fusion complexes are large, shallow, and hydrophobic, complex peptides such as those derived from the HR regions of gp41 are more effective inhibitory ligands than small molecules. Thus, for the last fifteen years, there has been an intensive and ongoing effort to develop synthetic constraints (13–17) or mutagenesis approaches (18–24) that fortify the natural helical structure of gp41 peptide sequences (9, 25–27) to maximize the pharmacologic potential of inhibiting viral fusion. To date, a synthetic design that accomplishes structural stabilization, neutral and acid protease resistance, enhanced antiviral efficacy, activity against resistant strains, and improved pharmacokinetic behavior that includes oral absorption, has not been achieved. Here, we report the application of hydrocarbon double-stapling to redress the biophysical and pharmacologic liabilities of a lengthy peptide therapeutic.

Results

Hydrocarbon Double-Stapling Fortifies Natural Peptide Therapeutics. Synthetic optimization of the HR2 fusion domain of gp41 has remained a pressing research goal since the successful development of enfuvirtide as an HIV-1 pharmaceutical (18–20). Whereas clin-

Author contributions: G.H.B., N.M., J.G. Supko, J.G.Sodroski, and L.D.W. designed research; G.H.B., N.M., A.F.P., A.M.P, J.G. Supko, X.H., E.G., J.G. Sodroski, and L.D.W. performed research; G.H.B., N.M., E.G., J.G. Sodroski, and L.D.W. contributed new reagents/analytic tools; G.H.B., N.M., A.F.P., A.M.P., J.G. Supko, E.G., J.G. Sodroski, and L.D.W. analyzed data; and G.H.B., N.M., J.G. Supko, J.G. Sodroski, and L.D.W. wrote the paper.

Conflict of interest statement: L.D.W. is a consultant and scientific advisory board member for Aileron Therapeutics.

*This Direct Submission article had a prearranged editor.

[1]To whom correspondence should be addressed. E-mail: Loren_Walensky@dfci.harvard.edu.

This article contains supporting information online at www.pnas.org/lookup/suppl/doi:10.1073/pnas.1002713107/-/DCSupplemental.

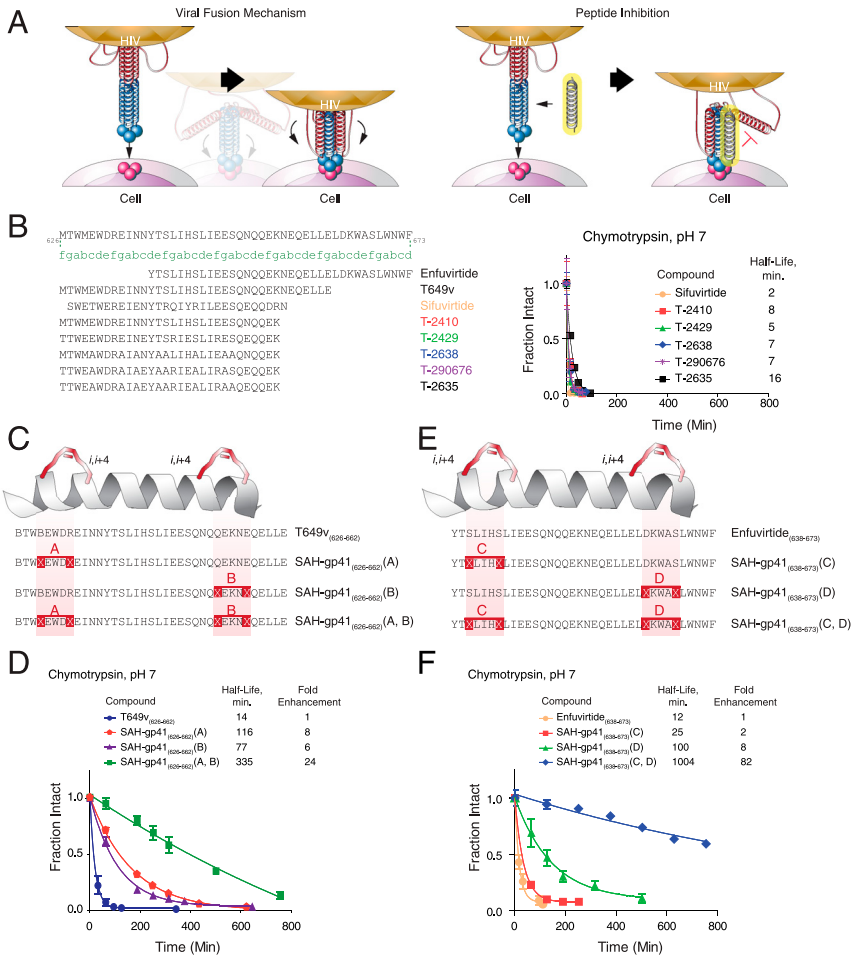

Fig. 1. Design and synthesis of SAH-gp41 peptides. (*A*) Schematic of the HIV-1 viral fusion mechanism and its disruption by a decoy HR2 helix. (*B*) A series of reported next-generation gp41 HR2 peptides (18, 20), which contain natural amino acid substitutions, helix-promoting alanine residues, and/or (i, $i+4$) salt bridges, exhibited rapid proteolytic degradation upon exposure to chymotrypsin. (*C*) SAH-gp41 peptides were designed based on gp41 HR2 domain sequences 626–662 (a variant of T649). X, substitution sites for crosslinking nonnatural amino acids; B, norleucine (substituted for methionine to optimize activity of the ruthenium catalyst). (*D*) Upon exposure to chymotrypsin, the singly stapled SAH-gp41 peptides exhibited 6–8-fold longer half-lives compared to the unmodified peptide, whereas double-stapling conferred a 24-fold enhancement in protease resistance. (*E*) Singly and doubly stapled SAH-gp41 peptides were also constructed based on the enfuvirtide peptide sequence (638–673). (*F*) Like SAH-gp41$_{(626–662)}$ peptides, the singly stapled SAH-gp41$_{(638–673)}$ derivatives showed enhanced chymotrypsin resistance compared to the template peptide, and the doubly stapled peptide was strikingly more resistant to proteolysis. Fraction intact, mean ± s.d.

ical enthusiasm for fusion inhibitors has waned due to the pharmacologic liabilities, the emergence of resistance, and their replacement by more effective therapeutic options, the mechanistic elegance of viral fusion inhibition and the potential broad application to preventing a host of viral infections, have continued to inspire basic and translational research in this arena. A variety of next-generation HIV-1 fusion inhibitor peptides with improved antiviral activity have been reported (18, 20, 28), yet the issue of proteolytic instability remains a potential concern, prompting the development of gp41-based peptides that replace portions of the natural alpha-amino acid backbone with protease-resistant D- or beta-amino acids (21, 29). However, can natural alpha-peptides be transformed into protease-resistant therapeutics by an alternate and broadly applicable approach?

To demonstrate the proteolytic challenges faced by enfuvirtide and its functionally optimized alpha-peptide derivatives (18, 20), we subjected a sampling of fusion inhibitors (25 μM) to in vitro chymotrypsin digestion (0.5 ng/μL, room temperature, pH 7) and monitored the kinetics of degradation by liquid chromatography/mass spectrometry (LC/MS) (Fig. 1*B*). In each case, rapid proteolysis was observed with calculated half-lives ranging from 2–16 min. In an effort to fortify HIV-1 fusion peptides, we inserted chemical staples at the N- or C-termini of T649v by substituting (*S*)-2-(((9*H*-fluoren-9-yl)methoxy)carbonylamino)-2-methyl-hept-6-enoic acid at select (i, $i+4$) positions, followed by ruthenium-catalyzed olefin metathesis (Fig. 1*C*). Sites for nonnatural amino acid insertion were carefully selected to avoid disruption of the critical hydrophobic interface between HR1 and HR2 helices as delineated by the crystal structure of gp41 (25). Because gp41 HR2 peptides are considerably longer than those previously subjected to hydrocarbon stapling (3, 5, 6, 30), we explored the synthetic feasibility and biophysical impact of "double-stapling" by inserting chemical staples at both N- and C-terminal positions (Fig. 1*C*). To achieve this synthetic goal, two pairs of (i, $i+4$) substitutions were made, ensuring a sufficient distance between nonnatural amino acid couples to avoid cross-reactivity upon olefin metathesis. Simply by extending the duration of synthetic coupling times for each nonnatural amino acid and its subsequent residue, the doubly stapled amphipathic peptide was successfully synthesized with similar high efficiency, purity (e.g., crude > 85%, HPLC-purified 98%), and solubility (e.g., 0.5 mM, D5W pH 8.5) as the corresponding unmodified peptide (Fig. S1), highlighting the capacity of the hydrocarbon stapling methodology to generate longer peptides with multiple chemical reinforcements.

When subjected to chymotrypsin, the singly stapled SAH-gp41$_{(626–662)}$ peptides displayed longer half-lives that ranged from 77–116 min, reflecting a 6–8-fold enhancement in chymotrypsin resistance compared to the corresponding unmodified peptide (Fig. 1*D*). Strikingly, the doubly stapled derivative exhibited a half-life of 335 min, surpassing the unmodified peptide by 24-fold and the singly stapled peptides by 3–4-fold (Fig. 1*D*). To determine if the impact of peptide double-stapling is manifest across diverse lengthy templates, we also generated singly and doubly stapled analogs of enfuvirtide (Fig. 1*E*) and exenatide (Byetta) (Fig. S2*A*), two US Food and Drug Administration approved peptide therapeutics for HIV-1 infection and diabetes, respectively. In each case, the singly stapled peptides displayed longer half-lives than their unmodified counterparts, and the doubly stapled peptides again exhibited even more dramatic protease resistance (Fig. 1*F* and Fig. S2*B*). Thus, a consistent pattern emerged whereby double-stapling conferred robust proteolytic

stability to the natural peptides and significantly outperformed single-stapling in the context of a lengthy peptide template.

Mechanism of Doubly Stapled Peptide Fortification. What accounts for the proteolytic stabilization conferred by hydrocarbon double-stapling? We first examined the most simplistic potential explanation: elimination of cleavage sites as a result of 4-position nonnatural amino acid substitution. However, inspection of the amino acid sequences of T649v and its stapled analogs revealed that the number and location of chymotrypsin cleavage sites remained unchanged for each of the compositions (Fig. 2*A*).

Because proteases require that peptides adopt an extended conformation to hydrolyze amide bonds, reinforcing α-helical structure can render peptides protease-resistant, as we previously demonstrated for singly stapled peptides (3, 5, 6). Could adding a second staple to a lengthy peptide be maximizing protease resistance by incrementally enhancing overall α-helical structure? We performed CD to examine the impact of single- and double-stapling on T649v peptide α-helicity. Whereas each of the stapled derivatives exhibited enhanced peptide α-helicity compared to the unmodified template (13%), SAH-gp41$_{(626–662)}$(B) was the most α-helical (63%), SAH-gp41$_{(626–662)}$(A) was the least helical stapled peptide (25%), and the doubly stapled SAH-gp41$_{(626–662)}$(A, B) peptide displayed intermediate α-helicity (36%) (Fig. 2*B*). Based on these data and the corresponding analysis of stapled enfuvirtide analogs (Fig. 1*F* and Fig. S3), we conclude that the degree of overall α-helicity does not explain the superior proteolytic resistance of doubly stapled peptides.

We next examined whether the proteolytic resistance of doubly stapled peptides derived from the presence of the two all-hydrocarbon crosslinks generated by olefin metathesis or is simply the result of 4-place insertion of the helix-promoting, hydrophobic, α,α-disubstituted (but uncrosslinked) nonnatural amino acids. Thus, we compared the α-helicity and chymotrypsin resistance of SAH-gp41$_{(626–662)}$(A, B) with its unmetathesized analog, designated unstapled alpha-helix (UAH)-gp41$_{(626–662)}$(A, B). We first noted that the overall α-helical stabilization afforded by inserting four α,α-disubstituted nonnatural amino acids was approximately the same whether the olefinic side chains were crosslinked or not (Fig. 2*B*). These data suggest that the α-helicity of SAH-gp41$_{(626–662)}$(A, B) is best predicted by the compatibility and resultant α-helical induction of the installed nonnatural amino acid pairs, rather than the α-helicities of the singly-stapled peptides (Fig. 2*B*). Strikingly, and despite the nearly identical CD profiles of SAH-gp41$_{(626–662)}$(A, B) and UAH-gp41$_{(626–662)}$(A, B), the unmetathesized construct is rapidly degraded, exhibiting a half-life 2–3-fold shorter than the corresponding singly stapled peptides (Fig. 1*D*) and 8-fold shorter than its doubly stapled counterpart (Fig. 2*C*). These data indicate that the covalent crosslinks themselves, rather than overall α-helicity or the incremental hydrophobicity conferred by 4-place substitution of the nonnatural amino acids, accounts for the protease-resistance feature of double-stapling.

Could the dramatic improvement in proteolytic stability of the doubly stapled peptide derive from peptide aggregation? Although it has already been reported that singly stapled peptides are monomeric at the micromolar concentrations employed for CD and proteolysis experiments (3, 31), we interrogated whether doubly stapled peptides were prone to aggregation. First, we employed CD across a broad temperature range to compare the melting curves of SAH-gp41$_{(626–662)}$(A, B) and its unmetathesized derivative UAH-gp41$_{(626–662)}$(A, B), and found that both peptides display similar, reversible, and cooperative unfolding profiles (Fig. 2*D*). After cooling, repeat temperature scanning revealed nearly identical melting curves, indicating that neither peptide is prone to aggregation and precipitation even at the supraphysiologic micromolar concentrations required to conduct the CD and proteolysis studies (Fig. 2*D*). Thus, whereas the two peptides have similar compositions, overall α-helicity, and melting profiles, they exhibit dramatically different chymotrypsin susceptibilities that can only be attributed to the presence or absence of the covalent crosslinks themselves. In further support of the monomeric status of the doubly stapled peptide, we observed that SAH-gp41$_{(626–662)}$(A, B) migrates as a monomer on native gel electrophoresis (Fig. S4) and elutes as a monomer by gel filtration analysis (Fig. S5).

To directly interrogate the effect of double-stapling on proteolytic cleavage of the template peptide, we used LC/MS to identify the proteolytic fragments generated by digesting the panel of peptides with chymotrypsin. Of the predicted proteolytic sites (Fig. 2*A*), the unmodified T649v was cleaved at four major locations (Fig. 2*E*). The C-terminal singly stapled peptide SAH-gp41$_{(626–662)}$(B) also showed cleavage at these four sites, but the timecourse for degradation was significantly prolonged compared to that of the unmodified peptide (Fig. 1*D*). The degradation pattern of the N-terminal singly stapled peptide SAH-gp41$_{(626–662)}$(A) demonstrated cleavage at the two C-terminal chymotrypsin sites but no cleavage was observed at the residues located within or just N-terminal to the $(i, i+4)$ crosslinked segment. These data reveal that insertion of a hydrocarbon staple in the immediate vicinity of peptidase cleavage sites explicitly prevents local proteolytic degradation. The cleavage pattern (Fig. 2*E*) and kinetics (Fig. 1*D*) of SAH-gp41$_{(626–662)}$(A, B) digestion demonstrate that the doubly stapled peptide manifests a synergistic benefit from the distinct antiproteolysis features of the individual staples, namely (1) delayed kinetics of degradation due to α-helical induction (C-terminal staple) and (2) complete blockade of proteolytic cleavage in the region of the installed

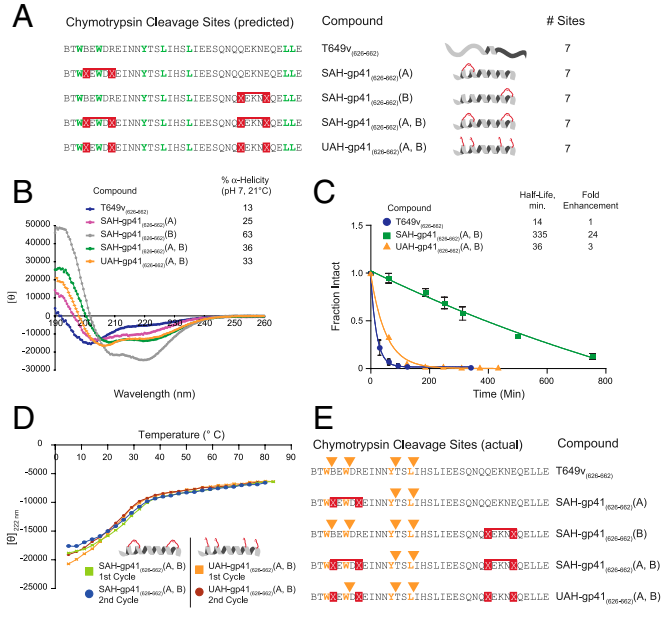

Fig. 2. Mechanistic analysis of peptide fortification by hydrocarbon double-stapling. (*A*) T649v and its synthetic derivatives contain the identical number of chymotrypsin cleavage sites. (*B*) CD demonstrated that T649v is predominantly a random coil in solution, whereas SAH-gp41$_{(626–662)}$ peptides exhibited varying degrees of increased α-helical content. UAH- and SAH-gp41$_{(626–662)}$ (A, B) displayed similar α-helical content, which was intermediate to that of the singly stapled peptides. (*C*) UAH-gp41$_{(626–662)}$(A, B) exhibited an 8-fold shorter half-life than its doubly stapled counterpart. Fraction intact, mean ± s.d. (*D*) UAH- and SAH-gp41$_{(626–662)}$(A, B) displayed similar melting profiles, with T_m values of 27 and 22 °C, respectively. Temperature-dependent unfolding was reversible for both peptides, as evidenced by the overlapping repeat melting curves. (*E*) Comparative chymotrypsin degradation patterns of T649v-based peptides. Of note, the N-terminal staple uniquely prevented proteolytic hydrolysis of the cleavage site flanked by the staple, with no corresponding $M + 18$ species observed by LC/MS.

covalent constraint (N-terminal staple). Comparative NMR analysis of T649v and SAH-gp41$_{(626–662)}$(A, B) revealed that the indole protons corresponding to the two N-terminal tryptophan residues in the vicinity of the staple were represented by two sharp peaks in the unmodified peptide, but were broadened and split in the doubly stapled peptide (Fig. S6). These NMR data are consistent with a discretely structured N-terminus in the doubly stapled peptide and fast exchange between multiple conformations in the unmodified peptide, rendering T649v susceptible to rapid proteolytic degradation. Whereas 4-place substitution of the α,α-disubstituted nonnatural amino acids dictates overall α-helical induction whether the residues are crosslinked by olefin metathesis or not, the cleavage pattern (Fig. 2*E*) and kinetics (Fig. 2*C*) of UAH-gp41$_{(626–662)}$(A, B) degradation demonstrate that the unstapled derivative lacks the dramatic antiproteolysis features of the stapled peptides, including the inability to block peptide cleavage at the site flanked by the N-terminal pair of (i, $i+4$)-substituted nonnatural amino acids.

Taken together, these data indicate that the proteolytic advantage conferred by peptide double-stapling does not derive from mutagenesis of protease cleavage sites, maximizing α-helicity alone, 4-place nonnatural amino substitution, or peptide aggregation. Instead, we determined that the striking protease resistance of doubly stapled peptides is conferred by a combination of (1) decreased rate of proteolysis due to induction of α-helical structure and (2) complete blockade of peptidase cleavage at sites localized within or immediately adjacent to the (i, $i+4$)-crosslinked segment.

Antiviral Activity of Doubly Stapled SAH-gp41$_{(626–662)}$ Peptide. In order for the antiproteolysis feature of double-stapling to have practical utility, doubly stapled peptides must retain at least equivalent biological activity to the parent wild-type peptide. To assess the functional impact of hydrocarbon double-stapling on gp41-based fusion inhibitor activity, SAH-gp41$_{(626–662)}$ peptides were tested and compared to T649v and enfuvirtide in a luciferase-based HIV-1 infectivity assay (32, 33), using virus with envelope glycoproteins derived from HXBc2 and the neutralization-resistant primary R5 isolate, YU2. All peptides demonstrated anti-HXBc2 activity, with the T649v-based constructs showing slightly superior efficacy compared to the enfuvirtide peptide generated either in our laboratory or by Trimeris (Fig. 3*A*). Of note, differences in potency among the unmodified and stapled T649v peptides were not apparent for HXBc2 due to its pan-sensitivity. However, for the neutralization-resistant primary YU2 isolate, SAH-gp41$_{(626–662)}$(A), SAH-gp41$_{(626–662)}$(B), and SAH-gp41$_{(626–662)}$(A, B) all demonstrated enhanced antiviral activity compared to enfuvirtide and T649v, with a rank order of (A,B) > (A) > (B) > T649v > enfuvirtide (Fig. 3*B*). The relative performance of SAH-gp41$_{(626–662)}$ peptides in this HIV-1 infectivity study indicated that maximizing overall α-helicity is not the sole biophysical determinant for optimizing fusion inhibition, consistent with conclusions from a prior study (16). Indeed, the doubly stapled peptide, which exhibits an intermediate α-helicity (Fig. 2*B*), appeared to strike the optimal balance, yielding a construct with both superior protease resistance and antiviral potency. Of note, none of the peptides tested demonstrated any activity against viruses with A-MLV envelope glycoproteins (Fig. S7), highlighting the functional specificity of SAH-gp41$_{(626–662)}$ peptides. In addition, the nanomolar range biological activity displayed by SAH-gp41$_{(626–662)}$(A, B) further emphasizes that the doubly stapled peptide functions as a monomer, because aggregation-prone HR2 peptides that display extreme thermal stability have markedly diminished antiviral activity due to a relative paucity of bioactive monomer (18).

An important requirement of next-generation viral fusion inhibitors is that they have the capacity to overcome enfuvirtide resistance mutations. We reasoned that by focally enforcing

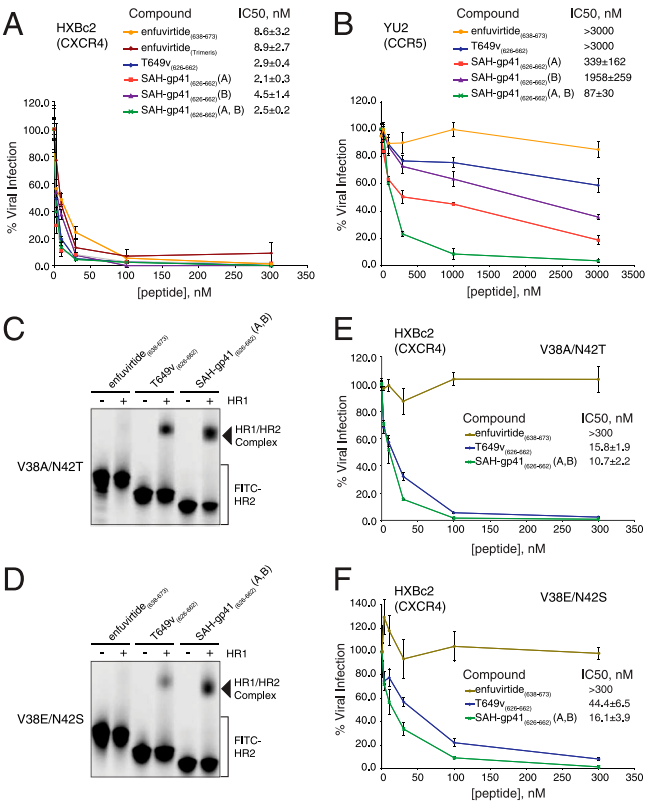

Fig. 3. Enhanced antiviral activity of SAH-gp41$_{(626–662)}$(A, B). (*A*) The gp41 HR2-derived peptides all blocked HXBc2 infectivity, with the T649v-based constructs showing slightly superior activity compared to enfuvirtide. (*B*) Singly and doubly stapled SAH-gp41$_{(626–662)}$ peptides demonstrated enhanced blockade of a neutralization-resistant virus that contains the YU2 envelope glycoproteins, with SAH-gp41$_{(626–662)}$(A, B) exhibiting the most potent antiviral activity. SAH-gp41$_{(626–662)}$(A, B) outperformed enfuvirtide and T649v in HR1/HR2 complex assembly (*C*, *D*) and infectivity assays (*E*, *F*) that respectively employed peptides and recombinant HIV-1 constructs bearing HR1 enfuvirtide-resistance mutations. % viral infection, mean ± s.e.m; IC50, mean ± s.d.

α-helical structure and decreasing the entropic cost of target binding, constrained HR2 peptides may sustain less impact from isolated gp41 resistance mutations. To test this hypothesis, we compared the functional activities of enfuvirtide, T649v, and SAH-gp41$_{(626–662)}$(A, B) in complex assembly and HIV-1 infectivity assays using peptides and recombinant HIV-1 HXBc2 virus bearing the HR1 double mutations V38A/N42T and V38E/N42S (19). Both mutants support HIV-1 entry with differential efficiencies but remain comparable to the wild-type virus. The mechanistic basis for their resistance instead derives from blockade of enfuvirtide binding, which is required for the peptide's dominant-negative activity in preventing gp41 six-helix bundle assembly. We first performed a native PAGE-based assay designed to monitor the capacity of FITC-HR2 and mutant HR1 peptides to interact to form a stable higher-order complex (28). Whereas FITC-labeled enfuvirtide showed no interactions with the doubly mutant HR1 peptides, FITC-T649v and FITC-SAH-gp41$_{(626–662)}$(A, B) formed a higher-order complex with each of the mutant HR1 peptides (Fig. 3 *C* and *D*). As evidenced by the fluorescence scans and the corresponding densitometric analyses, FITC-SAH-gp41$_{(626–662)}$(A, B) bound effectively to the doubly mutant HR1 peptides, even exhibiting up to 2-fold enhancement in binding activity compared to FITC-T649v (Fig. 3 *C* and *D*, and Fig. S8). In infectivity assays that employed HIV-1 HXBc2 envelope constructs bearing the corresponding gp41 HR1 mutations, enfuvirtide again showed no functional activity, whereas T649v and SAH-gp41$_{(626–662)}$(A, B) dose-responsively suppressed

HIV-1 infectivity (Fig. 3 *E* and *F*). Consistent with the native PAGE binding analysis, SAH-gp41$_{(626–662)}$(A, B) effectively blocked viral infectivity, displaying a 1.5–2.8-fold improvement over T649v in overcoming mutations that uniformly abrogate enfuvirtide activity in humans.

Favorable Pharmacokinetics of Doubly Stapled SAH-gp41$_{(626–662)}$ Peptide. We next examined whether the striking protease resistance observed for SAH-gp41$_{(626–662)}$(A, B) in vitro translated into a more advantageous pattern of systemic exposure in vivo. The pharmacokinetic behavior of T649v and SAH-gp41$_{(626–662)}$ (A, B) was comparatively evaluated in mice. Mice were injected intravenously with 10 mg/kg of the two peptides, blood was withdrawn after 5, 30, 60, 120, and 240 min (3 animals at each time point), and the concentration of the intact peptides in plasma was determined by LC/MS analysis. Inspection of the plasma concentration-time profiles for the T649v and SAH-gp41$_{(626–662)}$(A, B) peptides revealed a notable difference in the disposition of the two peptides (Fig. 4*A*). In particular, the maximum concentration in plasma (mean ± s.d.) observed in the initial sample obtained 5 min after dosing was 140 ± 13 μg/mL for SAH-gp41$_{(626–662)}$ (A, B) as compared to 32 ± 6 μg/mL for T649v, and the concentration of the doubly stapled peptide ranged from 4–23× greater than the unmodified peptide at each sample time. Although the time courses of both peptides appeared to be polyexponential, T649v could only be monitored for 2 h after dosing and it became undetectable before the apparent terminal disposition phase was achieved, precluding an estimation of its biological half-life. In contrast, the concentration of SAH-gp41$_{(626–662)}$(A, B) in plasma remained well above the 1.25 μg/mL limit of quantitation of the analytical method at 4 h and the half-life of the well-defined log-linear terminal phase of the plasma profile was 1.7 h. The area under the plasma concentration-time curve from time zero to infinity, which is a measure of the total systemic exposure to a drug, was 9,870 μg · min/mL for SAH-gp41$_{(626–662)}$(A, B) as compared to 1,050 μg · min/mL for T649v. Consequently, the total body clearance of the unmodified T649v peptide (9.5 mL/min/kg) was approximately 10× greater than that of SAH-gp41$_{(626–662)}$(A, B) (1.0 mL/min/kg). Thus, peptide double-stapling markedly enhanced the extent and duration of systemic exposure, redressing a key pharmacokinetic deficiency of HIV-1 fusion inhibitor peptides.

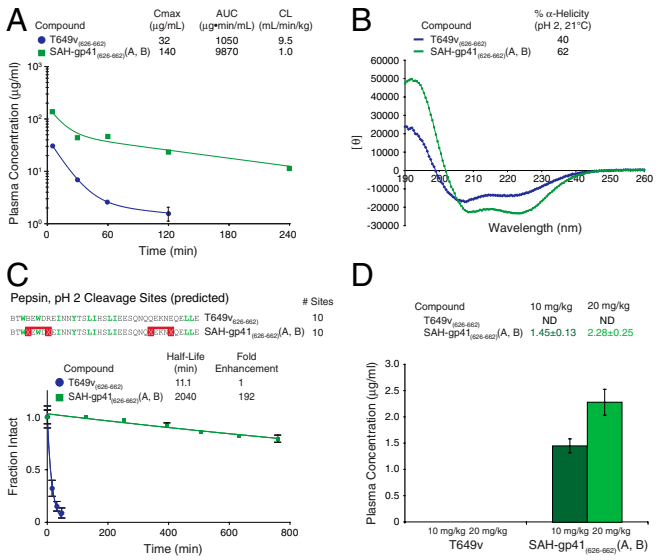

Fig. 4. Effect of double-stapling on pharmacokinetic behavior, acid protease resistance, and oral absorption. (*A*) Plasma concentrations of intact SAH-gp41$_{(626–662)}$(A, B) and T649v in mice treated by intravenous bolus injection. (*B*) CD revealed that SAH-gp41$_{(626–662)}$(A, B) exhibits even greater α-helicity at pH 2, surpassing T649v. (*C*) Upon exposure to pepsin at pH 2, T649v was rapidly degraded but SAH-gp41$_{(626–662)}$(A, B) was strikingly resistant. (*D*) Orally administered SAH-gp41$_{(626–662)}$(A, B) achieved measurable and dose-dependent plasma concentrations, whereas T649v was not detectable. Plasma concentration, mean ± s.d.; fraction intact, mean ± s.d.

Acid Protease Resistance and Oral Absorption of Doubly Stapled SAH-gp41$_{(626–662)}$ Peptide. Peptides have poor oral bioavailability due to rapid degradation in the proximal digestive tract. The compelling protease resistance of doubly stapled SAH-gp41$_{(626–662)}$ (A, B) peptide at neutral pH prompted us to compare the stability of T649v and SAH-gp41$_{(626–662)}$(A, B) under acidic conditions. Acidification of the peptide solutions significantly enhanced α-helical content, with SAH-gp41$_{(626–662)}$(A, B) maintaining greater α-helicity than T649v (Fig. 4*B*). Upon exposure to pepsin at 0.5 ng/μL, T649v exhibited rapid degradation, with a half-life of 11 min (Fig. 4*C*). Despite having the same number of pepsin cleavage sites, SAH-gp41$_{(626–662)}$(A, B) displayed a half-life nearly 200-fold longer than T649v and remained 80% intact after exposure to pepsin at pH 2 for >12 h (Fig. 4*C*). Indeed, the relative protease resistance observed among unmodified, singly, and doubly stapled T649v and enfuvirtide peptides at neutral pH (Fig. 1 *D* and *F*) was recapitulated under acidic conditions (Fig. S9). Given the remarkable pepsin resistance of SAH-gp41$_{(626–662)}$ (A, B), a pilot study was undertaken to compare the relative oral absorption of T649v and SAH-gp41$_{(626–662)}$(A, B). Mice were treated with single 10 and 20 mg/kg doses of T649v or SAH-gp41$_{(626–662)}$(A, B) in aqueous 5% dextrose (D5W) by oral gavage (3 animals per dose) and blood was collected by retroorbital bleed at 30 min after dosing. Measurable concentrations of the full-length peptide were found in plasma samples from all SAH-gp41$_{(626–662)}$(A, B) treated animals after oral dosing. In addition, the mean concentration of the peptide in plasma was dose-dependent (Fig. 4*D*). In contrast, T649v was undetectable in samples from all treated animals, irrespective of dosing level. Evidence of systemic levels of SAH-gp41$_{(626–662)}$(A, B) in mice after oral administration, although relatively low, demonstrates the potential for delivering stapled peptides by the oral route and warrants further investigation in primates.

Discussion

The helix–helix interfaces of gp41 constitute a validated target for HIV-1 fusion inhibition yet, like many protein–protein interactions, have proven challenging for small molecule development, reflecting a binding groove that is shallow, extensive, and complex. The sheer size and chemical diversity afforded by natural peptides have led to effective pharmacologic blockade of HIV-1 fusion by gp41 HR2-derived peptides. Theoretically, the mechanism of action of fusion inhibitors is ideally suited for front-line prevention of HIV-1 and other viral infections, yet the clinical application of enfuvirtide has been relegated to last line suppressive therapy as a result of the classical biophysical shortcomings of peptide therapeutics. For example, loss of bioactive structure, proteolytic lability, and the subcutaneous route of delivery are among the obstacles faced by peptide fusion inhibitors. Because enfuvirtide is nevertheless an effective targeted therapy for HIV-1 infection and paradigmatic of the obstacles faced by developmental peptide therapeutics, we evaluated hydrocarbon stapling as a remedy for the pharmacologic deficiencies of lengthy peptides.

We previously applied the hydrocarbon stapling methodology to develop cell-permeable bioactive helices for modulating apoptotic (5, 30) and transcriptional pathways (6). Here, we harnessed the technology to target an extracellular α-helical interaction that is fundamental to HIV-1 pathogenesis, and in doing so, generated the longest hydrocarbon stapled peptide helix synthesized to date. As HIV-1 fusion inhibitor peptides comprise 10 α-helical turns, we explored the feasibility and effectiveness of installing a second staple in an effort to extend the advantages of structural reinfor-

BIOCHEMISTRY

cement across a longer polypeptide distance. Indeed, we find that insertion of an additional staple is readily achievable from a synthetic standpoint and that the resultant peptides exhibit striking protease resistance at both neutral and acidic pH. The antiproteolysis feature of double-stapling extended to a variety of lengthy peptide templates, conferring chymotrypsin stability to T649v, enfuvirtide, and exenatide peptides, and far exceeded the performance of the corresponding singly stapled and unmodified peptides. A battery of synthetic and biophysical analyses ruled out protease cleavage site mutagenesis, α-helical stabilization alone, nonnatural amino acid substitution, and peptide aggregation as the source of peptide stabilization by double-stapling. Instead, the hydrocarbon double-staples themselves create a proteolytic shield both by slowing the kinetics of degradation through induction of α-helical structure and by explicitly preventing proteolysis at cleavage sites localized in the immediate vicinity of the staple. Importantly, doubly stapled SAH-gp41$_{(626–662)}$(A, B) exhibited improved activity against neutralization-resistant HIV-1 virus compared to the corresponding singly stapled and unmodified peptides, and even surmounted enfuvirtide resistance mutations. Finally, the clinical translation potential of hydrocarbon double-stapling is underscored by the enhanced pharmacokinetics of SAH-gp41$_{(626–662)}$(A, B), including the preliminary observation that oral absorption of a lengthy double-stapled peptide is achievable.

The potential broad applicability of the double-stapling approach beyond HIV-1 inhibition is exemplified by the wide variety of viral families that employ the six-helix bundle fusion mechanism for host infection, including Filovirus (e.g., Ebola) (34), Orthomyxovirus (e.g., influenza) (35), Coronavirus [e.g., Severe Acute Respiratory Syndrome (SARS)] (36), and Paramyxovirus [e.g., Respiratory Syncytial Virus (RSV)] (37). Indeed, the helix–helix interactions of the viral fusion apparatus represent a general target for preventive and suppressive antiviral agents. Whereas the practical challenges faced by enfuvirtide have served as a legitimate barrier to expanding the repertoire of peptide-based fusion inhibitors, their facile optimization by incorporation of hydrocarbon double-staples may unlock the therapeutic potential of this targeted antiviral strategy and perhaps other pharmacologic applications of lengthy peptides.

Methods

Peptide synthesis and characterization, HIV-1 infectivity and native PAGE assays, and pharmacokinetic studies were performed as described in detail in *SI Text*.

ACKNOWLEDGMENTS. We thank E. Smith for editorial and graphics assistance, and J. Fisher and J. Quijada for technical support in conducting the mouse pharmacokinetic studies. This work was supported by National Institutes of Health Grant 5F32 AI077371 (G.H.B.) and a Harvard Catalyst pilot grant and a Bill and Melinda Gates Foundation Grand Challenges Exploration award (L.D.W.).

1. Blackwell HE, Grubbs RH (1998) Highly efficient synthesis of covalently cross-linked peptide helices by ring-closing metathesis. *Angew Chem Int Edit* 37:3281–3284.
2. Blackwell HE, et al. (2001) Ring-closing metathesis of olefinic peptides: Design, synthesis, and structural characterization of macrocyclic helical peptides. *J Org Chem* 66:5291–5302.
3. Schafmeister CE, Po J, Verdine GL (2000) An all-hydrocarbon cross-linking system for enhancing the helicity and metabolic stability of peptides. *J Am Chem Soc* 122:5891–5892.
4. Bird GH, Bernal F, Pitter K, Walensky LD (2008) Synthesis and biophysical characterization of stabilized alpha-helices of BCL-2 domains. *Methods Enzymol* 446:369–386.
5. Walensky LD, et al. (2004) Activation of apoptosis in vivo by a hydrocarbon-stapled BH3 helix. *Science* 305:1466–1470.
6. Bernal F, Tyler AF, Korsmeyer SJ, Walensky LD, Verdine GL (2007) Reactivation of the p53 tumor suppressor pathway by a stapled p53 peptide. *J Am Chem Soc* 129:2456–2457.
7. Kilby JM, et al. (1998) Potent suppression of HIV-1 replication in humans by T-20, a peptide inhibitor of gp41-mediated virus entry. *Nat Med* 4:1302–1307.
8. Chan DC, Chutkowski CT, Kim PS (1998) Evidence that a prominent cavity in the coiled coil of HIV type 1 gp41 is an attractive drug target. *Proc Natl Acad Sci USA* 95:15613–15617.
9. Weissenhorn W, Dessen A, Harrison SC, Skehel JJ, Wiley DC (1997) Atomic structure of the ectodomain from HIV-1 gp41. *Nature* 387:426–430.
10. Kilby JM, et al. (2002) The safety, plasma pharmacokinetics, and antiviral activity of subcutaneous enfuvirtide (T-20), a peptide inhibitor of gp41-mediated virus fusion, in HIV-infected adults. *AIDS Res Hum Retroviruses* 18:685–693.
11. Wei XP, et al. (2002) Emergence of resistant human immunodeficiency virus type 1 in patients receiving fusion inhibitor (T-20) monotherapy. *Antimicrob Agents Chemother* 46:1896–1905.
12. Rimsky LT, Shugars DC, Matthews TJ (1998) Determinants of human immunodeficiency virus type 1 resistance to gp41-derived inhibitory peptides. *J Virol* 72:986–993.
13. Brunel FM, Dawson PE (2005) Synthesis of constrained helical peptides by thioether ligation: application to analogs of gp41. *Chem Commun* 20:2552–2554.
14. Judice JK, et al. (1997) Inhibition of HIV type 1 infectivity by constrained alpha -helical peptides: Implications for the viral fusion mechanism. *Proc Natl Acad Sci USA* 94:13426–13430.
15. Lee MK, Kim HK, Lee TY, Hahm KS, Kim KL (2006) Structure-activity relationships of anti-HIV-1 peptides with disulfide linkage between D- and L-cysteine at positions *i* and *i* + 3, respectively, derived from HIV-1 gp41 C-peptide. *Exp Mol Med* 38:18–26.
16. Sia SK, Carr PA, Cochran AG, Malashkevich VN, Kim PS (2002) Short constrained peptides that inhibit HIV-1 entry. *Proc Natl Acad Sci USA* 99:14664–14669.
17. Wang D, Lu M, Arora PS (2008) Inhibition of HIV-1 fusion by hydrogen-bond-surrogate-based alpha helices. *Angew Chem Int Edit* 47:1879–1882.
18. Dwyer JJ, et al. (2007) Design of helical, oligomeric HIV-1 fusion inhibitor peptides with potent activity against enfuvirtide-resistant virus. *Proc Natl Acad Sci USA* 104:12772–12777.
19. He Y, et al. (2008) Potent HIV fusion inhibitors against Enfuvirtide-resistant HIV-1 strains. *Proc Natl Acad Sci USA* 105:16332–16337.
20. He Y, et al. (2008) Design and evaluation of sifuvirtide, a novel HIV-1 fusion inhibitor. *J Biol Chem* 283:11126–11134.
21. Horne WS, et al. (2009) Structural and biological mimicry of protein surface recognition by alpha/beta-peptide foldamers. *Proc Natl Acad Sci USA* 106:14751–14756.
22. Izumi K, et al. (2009) Design of peptide-based inhibitors for human immunodeficiency virus type 1 strains resistant to T-20. *J Biol Chem* 284:4914–4920.
23. Naito T, et al. (2009) SC29EK, a peptide fusion inhibitor with enhanced alpha-helicity, inhibits replication of human immunodeficiency virus type 1 mutants resistant to enfuvirtide. *Antimicrob Agents Chemother* 53:1013–1018.
24. Nishikawa H, et al. (2009) Electrostatically constrained alpha-helical peptide inhibits replication of HIV-1 resistant to enfuvirtide. *Int J Biochem Cell Biol* 41:891–899.
25. Chan DC, Fass D, Berger JM, Kim PS (1997) Core structure of gp41 from the HIV envelope glycoprotein. *Cell* 89:263–273.
26. Jiang SB, Lin K, Strick N, Neurath AR (1993) Hiv-1 Inhibition by a Peptide. *Nature* 365:113.
27. Wild C, Oas T, McDanal C, Bolognesi D, Matthews T (1992) A synthetic peptide inhibitor of human-immunodeficiency-virus replication—Correlation between solution structure and viral inhibition. *Proc Natl Acad Sci USA* 89:10537–10541.
28. He YX, et al. (2008) Potent HIV fusion inhibitors against Enfuvirtide-resistant HIV-1 strains. *Proc Natl Acad Sci USA* 105:16332–16337.
29. Welch BD, VanDemark AP, Heroux A, Hill CP, Kay MS (2007) Potent D-peptide inhibitors of HIV-1 entry. *Proc Natl Acad Sci USA* 104:16828–16833.
30. Walensky LD, et al. (2006) A stapled BID BH3 helix directly binds and activates BAX. *Mol Cell* 24:199–210.
31. Kutchukian PS, Yang JS, Verdine GL, Shakhnovich EI (2009) All-atom model for stabilization of alpha-helical structure in peptides by hydrocarbon staples. *J Am Chem Soc* 131:4622–4627.
32. Si ZH, Cayabyab M, Sodroski J (2001) Envelope glycoprotein determinants of neutralization resistance in a simian-human immunodeficiency virus (SHIV-HXBc2P 3.2) derived by passage in monkeys. *J Virol* 75:4208–4218.
33. Si ZH, et al. (2004) Small-molecule inhibitors of HIV-1 entry block receptor-induced conformational changes in the viral envelope glycoproteins. *Proc Natl Acad Sci USA* 101:5036–5041.
34. Weissenhorn W, Carfi A, Lee KH, Skehel JJ, Wiley DC (1998) Crystal structure of the Ebola virus membrane fusion subunit, GP2, from the envelope glycoprotein ectodomain. *Mol Cell* 2:605–616.
35. Bullough PA, Hughson FM, Skehel JJ, Wiley DC (1994) Structure of influenza haemagglutinin at the ph of membrane-fusion. *Nature* 371:37–43.
36. Xu YH, et al. (2004) Crystal structure of severe acute respiratory syndrome coronavirus spike protein fusion core. *J Biol Chem* 279:49414–49419.
37. Zhao X, Singh M, Malashkevich VN, Kim PS (2000) Structural characterization of the human respiratory syncytial virus fusion protein core. *Proc Natl Acad Sci USA* 97:14172–14177.